# 7.2 Numerical Simulation of a Nano-pulsed High-voltage Discharge and Impact on Low-temperature Plasma Ignition Processes for Automotive Applications

Riccardo Scarcelli, Sayan Biswas, Isaac Ekoto, Douglas Breden, Anand Karpatne, Laxminarayan Raja

## Abstract

Spark-ignition (SI) processes are facing some challenges with the SI engine research continuing to move towards extremely dilute operation. Typical response from the automotive OEMs is to increase the spark energy to hundreds of mJs. However, this approach reduces the spark-plug lifetime due to erosion. In recent years, several low-temperature plasma (LTP) technologies (e.g. microwave, nanosecond pulsed discharge, Corona discharge) have been proposed for automotive applications as a substitute for the conventional SI process, yet no LTP ignition models are available for commercial computational fluid dynamics (CFD) codes for the evaluation and optimization of these advanced ignition systems.

This paper summarizes recent efforts to model LTP generated by a nano-pulsed high-voltage discharge in a multi-dimensional fashion. Streamer discharges between two pin electrodes are modeled through 2-D computations using the non-equilibrium plasma commercial solver VizGlow. The impact of key parameters such as peak voltage and gas density on the characteristics of the streamers is evaluated. The experimental dataset is used to validate the numerical predictions in terms of thermal and chemical properties of the generated plasma at the end of the discharge. Then, the impact of the post-discharge characteristics on the LTP ignition process is evaluated in combustion simulations performed using the CFD code CONVERGE.

## Introduction

In the last decade, the performance of automotive spark-ignition (SI) engines has been continuously improved by means of the aggressive enhancement of several specific engine parameters, including intake pressure, in-cylinder turbulence, compression ratio, and exhaust gas recirculation (EGR), leading to the demonstration of 40-45% brake thermal efficiency for gasoline SI engines [1],[2]. However, current ignition strategies for high-efficiency engines still rely mostly on the conventional spark-plug technology. Elevated spark energy values (hundreds of mJs) can improve combustion stability at more dilute operating conditions, but also accelerate electrode erosion rates that ultimately shorten spark-plug lifetimes.

In the last few years, low-temperature plasma (LTP) devices have shown the potential to enhance ignition and eliminate many of the issues related to spark-delivered thermal plasma such as heat losses, erosion, and material ablation [3]. SI engine testing using a nano-pulsed high-voltage discharge has demonstrated that it is possible to extend the EGR dilution tolerance with respect to conventional spark-plugs [4]. However, the

LTP characteristics and the ignition mechanism from LTP in an engine are poorly understood, creating a major barrier for development, optimization, and practical application to internal combustion engines (ICEs).

What stands out in the engine CFD community is that there are no models available to simulate LTP ignition, and this negatively affect the research on such non-conventional technique applied to ICEs. Also, most of the plasma assisted ignition (PAI) research community focuses on below-atmosphere or atmospheric plasmas [5], with 0-D global reactor studies of the plasma-combustion chemistry enhancements [6]. However, at engine-like conditions, LTP becomes highly non-uniform in space, and the plasma characteristics can vary significantly in the gap region between the electrodes.

This paper aims at modeling the non-equilibrium plasma generated by a pulsed nanosecond discharge in a high-fidelity, multi-dimensional fashion and providing quantification of the chemical and thermal properties of the plasma. Simulations are validated through experimental data obtained from calorimetry combined with advanced diagnostics. The impact of plasma properties on ignition processes at low temperature is the evaluated through CFD combustion calculations that use detailed kinetics.

# 1 Numerical Model

## 1.1 Simulation Approach

In this paper, both non-equilibrium plasma 2-D simulations and CFD combustion 3-D simulations are performed. Figure 1 shows the computational domain simulated with VizGlow and CONVERGE, used for non-equilibrium plasma 2-D simulations and CFD combustion 3-D simulations respectively. The test case geometry of interest consists of a pin-to-pin electrode configuration installed in an optically accessible calorimeter.

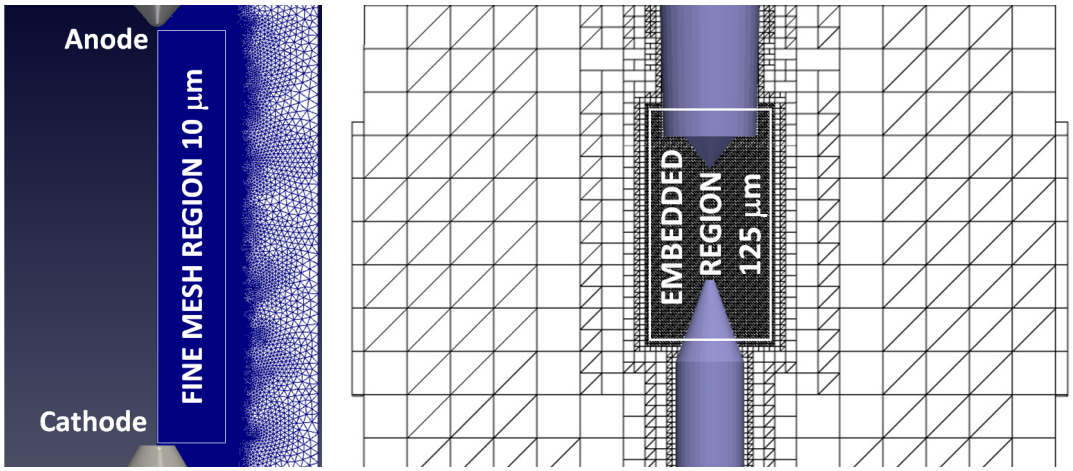


*Figure 1: Computational domain in VizGlow (left) and CONVERGE (right)*

Non-equilibrium plasma calculations are performed with VizGlow in the fluid region between the two electrodes, which corresponds only to a small portion of the entire calorimeter domain. The boundary conditions imposed in VizGlow consist of an axis-symmetric solution with respect to the axis between the two electrodes and open symmetry for the remaining fluid boundaries of the 2-D domain. The anode and cathode are defined as solid walls, with the electrical pulse (voltage) applied to the anode and

a fixed electrostatic potential condition used for the cathode. The inter-gap region (5.2 mm in length) is meshed with fine (10 μm) quadrilaterals. The mesh size quickly increases outside of the fine region, as indicated in Figure 1, through the adoption of triangle cells at increasing length. The total mesh count is 80,000.

CFD combustion calculations are performed with CONVERGE and simulate the entire calorimeter geometry. All the boundaries of the simulation domain are set to solid walls. A slice of the 3-D domain is shown in Figure 1 and emphasizes the use of embedding (fixed mesh refinement) to increase the mesh resolution (down to 125 μm) in the inter-gap region without significantly affecting the total cell count. Initial cell count is 200,000, but additional computational cells are introduced outside of the embedded region by means of the adaptive mesh refinement (AMR) algorithm implemented in CONVERGE, which is used to resolve velocity and temperature gradients across the flame. Maximum cell count of the CFD simulations is 300,000 as an effect of AMR.

To summarize the simulation approach followed in this study, 2-D non-equilibrium plasma simulations are performed first with VizGlow and leverage experimental data (voltage profile as boundary condition applied to the anode) to model the streamer discharge phase. 3-D CFD combustion simulations are performed next with CONVERGE and leverage the output from VizGlow to initialize the ignition calculations in the entire calorimeter domain.

## 1.2 Non-equilibrium plasma calculations

VizGlow is a general purpose self-consistent, multi-species, multi-temperature non-equilibrium plasma solver [7] that can be specialized to describe high-pressure corona, glow, or streamers discharge of interest. A number of governing equations are solved in conjunction with the Poisson's equation for the self-consistent electrostatic field in the plasma. These differential equations account for the production/destruction and transport of multiple charged and neutral species and the electron and bulk gas energy distribution. The photoionization mechanism is an important source of background electrons for the streamer propagation in air mixtures, and is also accounted for in the model. Species continuity equations are formulated as the following:

$$\frac{\partial \mathrm{n_k}}{\partial \mathrm{t}} + \vec{\nabla} \cdot \vec{\Gamma}_\mathrm{k} = \dot{\mathrm{G}}_\mathrm{k} \tag{1}$$

where k is the species index. All the involved species are solved except for one neutral species, which is the dominant background species. The gas chemistry source term $\dot{\mathrm{G}}_\mathrm{k}$ is calculated using a finite-rate chemistry mechanism. The number density of the dominant background is calculated based on ideal gas law at specified total gas pressure and gas temperature, by subtracting all other species handled by this species continuity equation. A plasma chemical kinetic mechanism for air is used in this study. The mechanism consists of a total of 18 species: E, $O_2$, $O_2$*, $O_2$a1, $O_2$b1, $O_2$+, $O_2$-, O, O-, $O_4$+, $O_2$+$N_2$, $N_2$, $N_2$a1, $N_2$A, $N_2$B, $N_2$C, $N_2$+, $N_4$+. Here, E is electrons, $O_2$* is the excited Herzberg state, $O_2$a1 is the singlet delta, and $O_2$b1 is a singlet sigma excited states of molecular oxygen, $N_2$a1, $N_2$A, $N_2$B, and $N_2$C are electronically states of molecular nitrogen, species symbols with "+" indicate positive ions, and "-" indicate negative ions. We also note cluster ions $O_4$+, $O_2$+$N_2$, and $N_4$+ that are stable forms. The species number flux term $\vec{\Gamma}_\mathrm{k}$ is obtained using the drift-diffusion approximation, which

is accurate at pressures of 100 mTorr and higher and at room temperature when the mean free path of the species (on order of μm) are much smaller than the characteristics length scales of the geometry (on order of mm). Electron energy transport is accounted for by solving the electron temperature using the electron energy conservation equation:

$$\frac{\partial e_e}{\partial t} + \vec{\nabla} \cdot \left( (e_e + p_e)\overrightarrow{u_e} - \kappa_e \vec{\nabla} T_e \right) = e\vec{\Gamma}_e \cdot \vec{\nabla}\,\phi - e\sum_i \Delta E_i^e r_i - \frac{3}{2} k_B n_e \frac{2m_e}{m_b}(T_e - T_g)\overline{\nu_e} \qquad (2)$$

The right-hand side of the electron energy equation incorporates three source terms: Joule heating, inelastic collisional heating, and elastic collisional heating, respectively. The bulk temperature is obtained by solving the energy conservation equation:

$$\frac{\partial e_h}{\partial t} + \vec{\nabla} \cdot \left( -\kappa_h \vec{\nabla} T_h \right) = \sum_k e Z_k \vec{\Gamma}_k \cdot \vec{\nabla}\,\phi + \frac{3}{2} k_B n_e \frac{2m_e}{m_b}(T_e - T_h)\overline{\nu_e} - e\sum_i \Delta E_i^h r_i \qquad (3)$$

The simulations performed in this study leverage the assumption that the bulk fluid motion is omitted, due to the small temporal scale of the discharge. Therefore, local mean velocity $\vec{u}_h$ is equal to zero and does not appear in Equation 3, while pressure is fixed. Additional details of the non-equilibrium plasma simulation methodology used in this study, including the full description of the plasma mechanism, can be found in literature [8].

### 1.3 CFD combustion calculations

The CFD ignition and combustion numerical simulations are performed with CONVERGE, release 2.3.17, a general-purpose computational fluid dynamics code that calculates incompressible or compressible, chemically-reacting fluid flows in complex three-dimensional geometries. CONVERGE's automated mesh generation based on modified cut-cell Cartesian method [9] helps to simplify the modeling process. Simple orthogonal Eulerian grids with embedded mesh refinements and AMR are used in this study. Continuity, momentum, and energy equations are solved and turbulence is modeled by the RNG k-ε RANS model. A well-stirred reactor combustion model (SAGE solver) with multi-zone approach and a 110 species iso-octane mechanism developed for low-pressure applications [10] are used in this study to simulate combustion. Modeling of heat transfer between fluid and solid is usually achieved by activating CHT modeling in CONVERGE. However, due to the short deposition (≈ 100 ns) and the low-temperature nature of the plasma, CHT calculations are not performed in this study and the electrode surfaces in CONVERGE are treated as boundaries with an imposed fixed temperature.

Simulation of ignition relies on mixed thermal energy and species deposition at the end of the plasma discharge. In the proposed numerical setup, there is no need to switch from ignition to combustion modeling. The mixed energy/species deposition has the effect of elevating the internal energy and increasing the concentration of reactants. Combustion is simulated through detailed chemistry with reaction rates defined in Arrhenius-form and therefore is automatically triggered by the increase of thermal and chemical energy imposed at each pulse. Up to 5 pulses are simulated in a mixture of air and iso-octane, in quiescent conditions, at an equivalence ratio of 1.0, with a pulse repetition rate of 10 kHz, equivalent to a dwell time of 100 μs.

There are two main assumptions made by the authors in this study: first, the results of the nano-pulsed discharge in a stoichiometric mixture of air and fuel (input to CONVERGE) are considered to be equivalent to the ones obtained in air only (output from VizGlow). This assumption is justified by the small concentration of the fuel with respect to air in a stoichiometric mixture. Secondly, in a train of pulses, the assumption is made that the results of the nanosecond pulsed discharge do not change from pulse to pulse. This assumption will have to be analyzed more in depth and verified, as it is known that the discharge regime could transition from glow into spark with the increase of number of pulses. However, the goal of this study is to demonstrate that LTP ignition can be practically simulated using conventional CFD engine tools, and the authors defer the development of an accurate LTP ignition model for multi-pulse applications to a later time.

## 2 Results

VizGlow simulations describe the streamer discharge between two pin electrodes when a high-voltage nanosecond pulse is delivered at the anode. Depending on the operating condition, the experimental voltage profiles feature a steep rise around t = 40-60 ns, peak at about t = 70-90 ns, and drop to zero after t = 150 ns. Figure 2 shows the evolution of the discharge on a temporal scale for a peak voltage value of 14 kV and an initial pressure of 1.5 bar (here referred as to case 1). Initial temperature in simulations, as well as in all experiments, is 70°C (343 K).

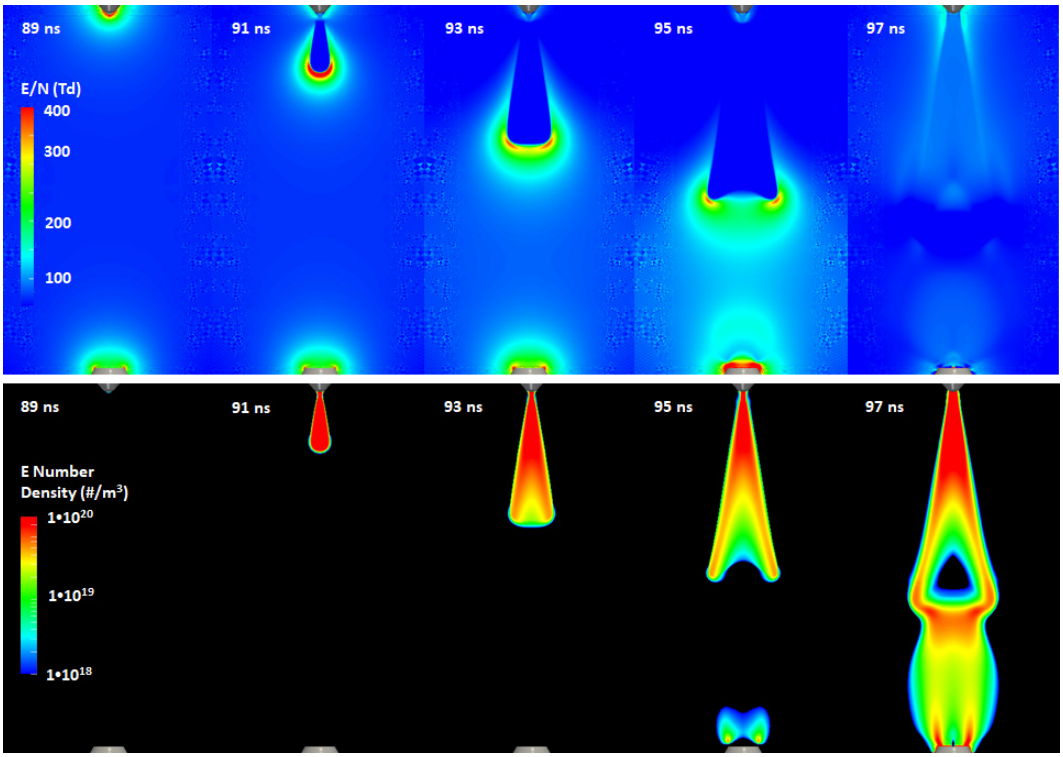


*Figure 2: Streamer induction and propagation for case 1 (14 kV, 1.5 bar)*

Positive and negative streamers are induced at the tip of both electrodes when the reduced electric field E/N, with N being the number density, becomes greater than the

breakdown field value. After induction, streamers quickly propagate towards the opposite electrode, and eventually bridge the gap in a very short (about 5 ns) time. Once the streamers bridge the gap, the plasma can remain in a glow (streamer) regime or transition to a spark regime depending on the characteristics of the inter-gap region, in particular the reduced electric field value. The operating condition shown in Figure 2 ultimately results in a glow discharge. When the voltage drops, the electrical current between the electrodes decreases and the spark is avoided.

Figure 3 shows the streamer formation and propagation at higher pressure and higher peak voltage values than case 1 (19 kV and 2.0 bar, here referred as to case 2). The timescales for case 2 are comparable with the ones for case 1, the slightly faster streamer induction being due to the shape of the voltage pulse for 19kV, which features a steeper increase than for 14 kV, resulting in the streamer induction occurring approximately 20 ns earlier. Both the reduced electric field and the electron number density distributions are similar to the ones for case 1, with the exception that case 2 shows an increased streamer branching due to the increased pressure in the gap. The streamers bridge the gap again in a very short timeframe, which is comparable with the one shown in case 1. Case 2 also does not transition into a spark and results into a true LTP condition.

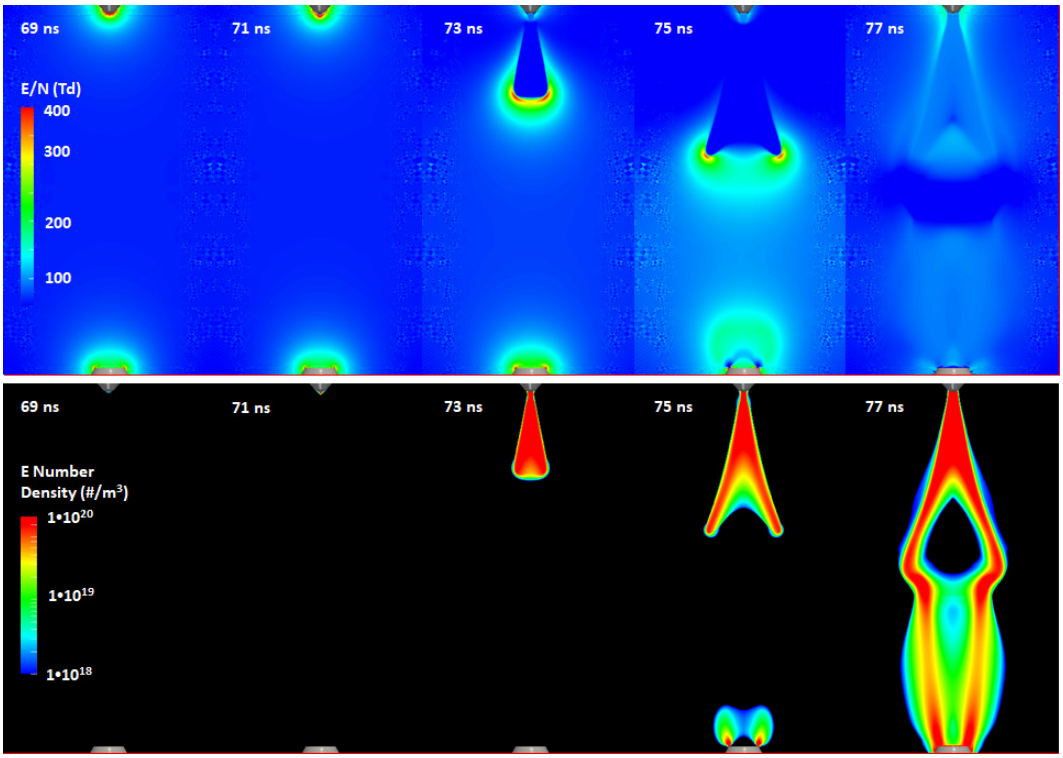


*Figure 3: Streamer induction and propagation for case 2 (19 kV, 2.0 bar)*

Figure 4 shows the characteristics of the non-equilibrium plasma for case 1 and case 2 at the end of the discharge (t = 150 ns), meaning after the voltage applied to the anode has dropped to zero. The chemical component of the plasma is represented by atomic oxygen O, while the thermal component is represented by temperature.

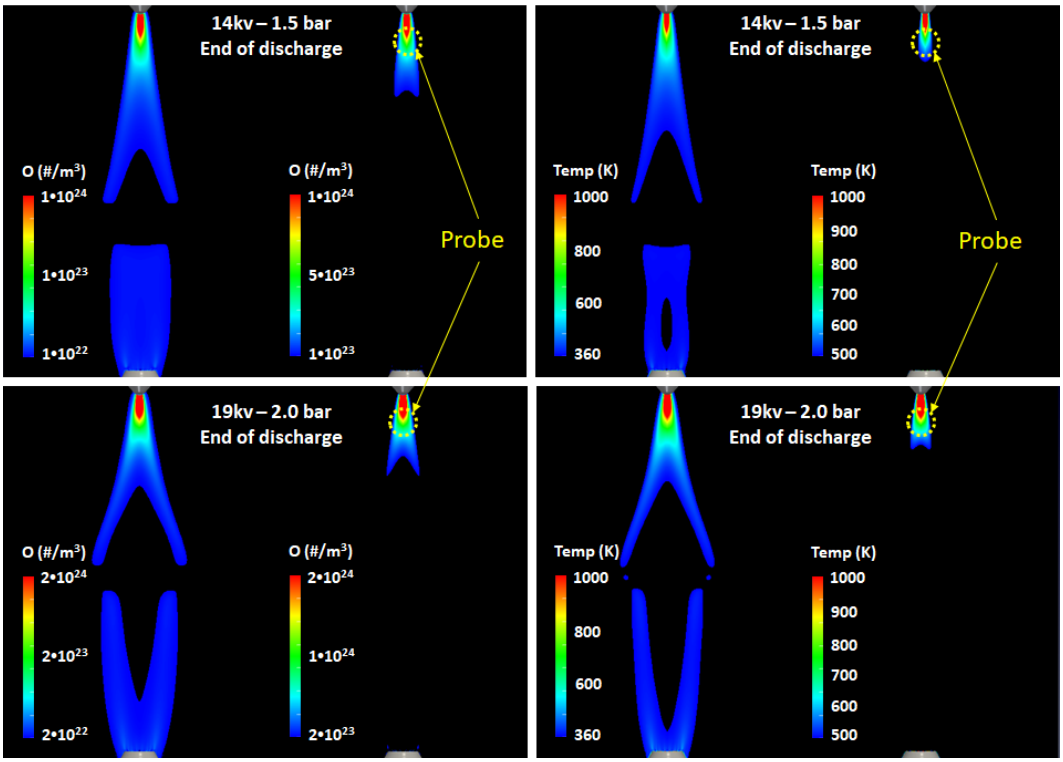


*Figure 4: O (left) and Temperature (right) distributions for case 1 (top) and case 2 (bottom). Both are shown using two different scales to emphasize local distributions*

It can be seen that, while the generation of atomic oxygen and the increase of temperature involve the entire region between the electrodes, the most relevant O generation and temperature increase are both observed in the close proximity of the anode only. This is due to the specific electrode geometry, which features a rounded tip shape with enhanced local electric field at the anode and a flat top surface, with consequent lower field enhancement, at the cathode. For the same reason, positive streamers (i.e. streamers directed to the cathode) are induced and start propagating earlier than negative streamers, as can be seen in both Figure 2 and Figure 3.

It is known that the location of the largest generation of active radicals and excited molecules is crucial to characterize, since the LTP ignition mechanism will be triggered first in that portion of the domain [11]. In Figure 4 it can be seen that such location is well defined by a conical frustum which has a length of approximately 1/8 of the total gap size. Figure 4 also shows the location of the experimental probe used for the quantitative O-TALIF measurements. Table 1 shows a comparison between simulation and experiments in terms of atomic oxygen produced in the proximity of the anode and temperature in the gap. Table 1 shows that the non-equilibrium plasma simulations closely match experimental data.

*Table 1: Comparison of plasma properties between modeling and experiments*

| | Simulation | | Experiment | |
|---|---|---|---|---|
| Test condition | O (1/cm$^3$) | T (K) | O (1/cm$^3$) | T (K) |
| 14.4 kV, 1.5 bar | 0.9 x 10$^{18}$ | 770 | 1.3 x 10$^{18}$ | 779 |
| 19.2 kV, 2.0 bar | 1.8 x 10$^{18}$ | 938 | 2.1 x 10$^{18}$ | 1094 |

Once the characteristics of the plasma calculated using simulations are validated against experimental data on quantitative basis, the impact of plasma properties on LTP ignition mechanism can be properly evaluated. Figure 5 shows how the thermal and non-thermal components of the plasma are taken into account. Both energy (which translates into temperature increase) and O species are deposited in a region that has the same size of the region shown in Figure 4 and that represents the part of the domain with the most significant increase of temperature and O concentration.

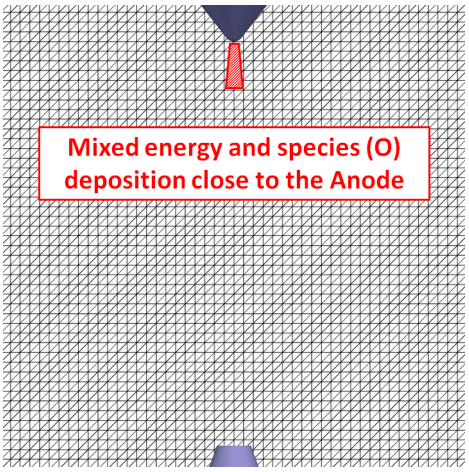


*Figure 5: Approach chosen to initialize ignition calculations in CONVERGE.*

The LTP discharge is simulated in a multi-pulse fashion. For both the two operating conditions evaluated in this paper, a number of subsequent pulses is simulated at a fixed pulse repetition rate, i.e. one pulse every 100 μs. The impact of the number of pulses on the modeled LTP ignition process is shown in Figure 6 and Figure 7.

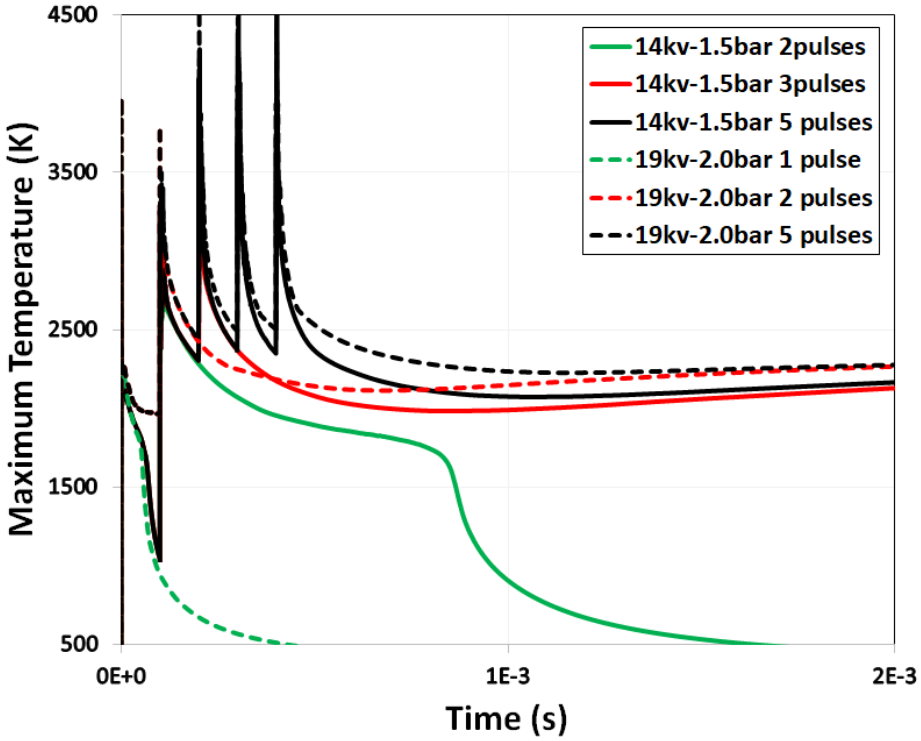


*Figure 6: Impact of number of pulses on maximum CFD temperature*

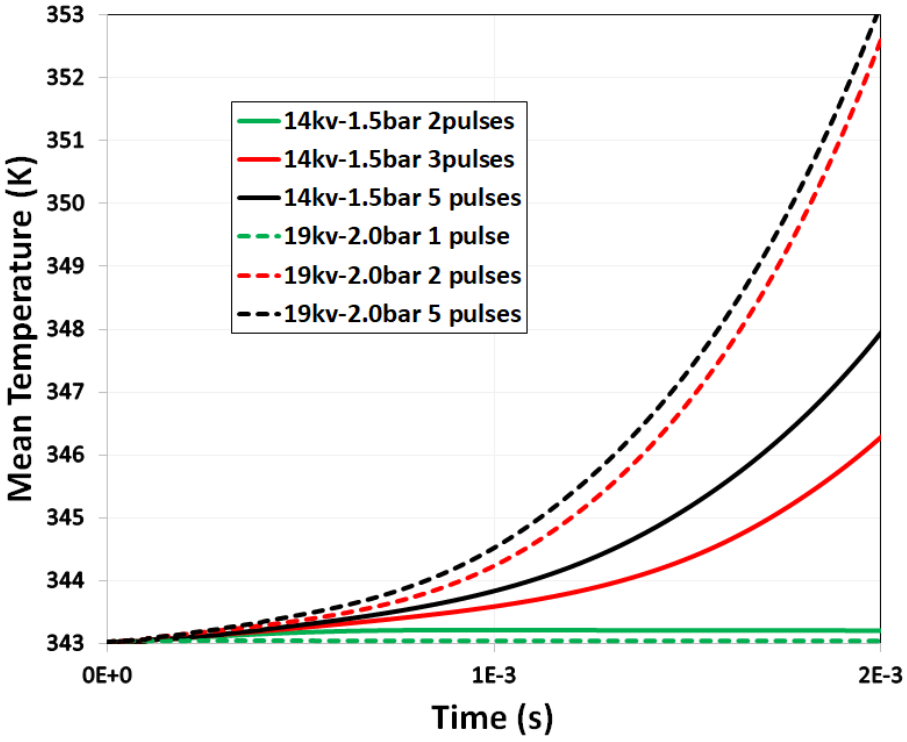


*Figure 7: Impact of number of pulses on mean CFD temperature*

Not shown in this paper, although a combined energy/species deposition is simulated, chemistry is activated by the low-temperature chemical component. Depositing a thermal energy that increases the local temperature to 800-1000 K alone is not capable of triggering the chemical reactions in a way that leads to self-sustained kinetics.

There is a clear effect of the number of pulses on mixture ignitability that can be observed looking at both the maximum (Figure 6) and mean (Figure 7) temperature values calculated in the full calorimeter CFD combustion cases. Case 1 (14 kV, 1.5 bar) requires at least 3 pulses to ignite, while case 2 (19 kV, 2.0 bar) requires at least 2 pulses. Also adding more pulses beyond a minimum required number does not seem to be decisive. In particular, case 2 features faster combustion than case 1. For case 2, applying 2 or 5 pulses does not make a significant difference.

This can also be observed in Figure 8 that shows the distribution of OH mass fraction for case 2, when 1 pulse, 2 pulses, or 5 pulses are applied to the electrodes. The amount of radicals generated with only 1 pulse is not sufficient to trigger chemical reaction in a self-sustained fashion. Adding one pulse will turn the discharge into a successful ignition process. From 3 pulses on, only limited benefits can be observed in the flame kernel growth. Nevertheless, it is worth pointing out that the specific operating condition is stoichiometric and is also evaluated at quiescent conditions. Under lean or dilute cases, and in presence of a non-quiescent flow conditions, a larger number of pulses could be required due to the low flame laminar speed and continuous displacement of the radicals that are deposited during the nano-pulsed discharge as an effect of the flow.

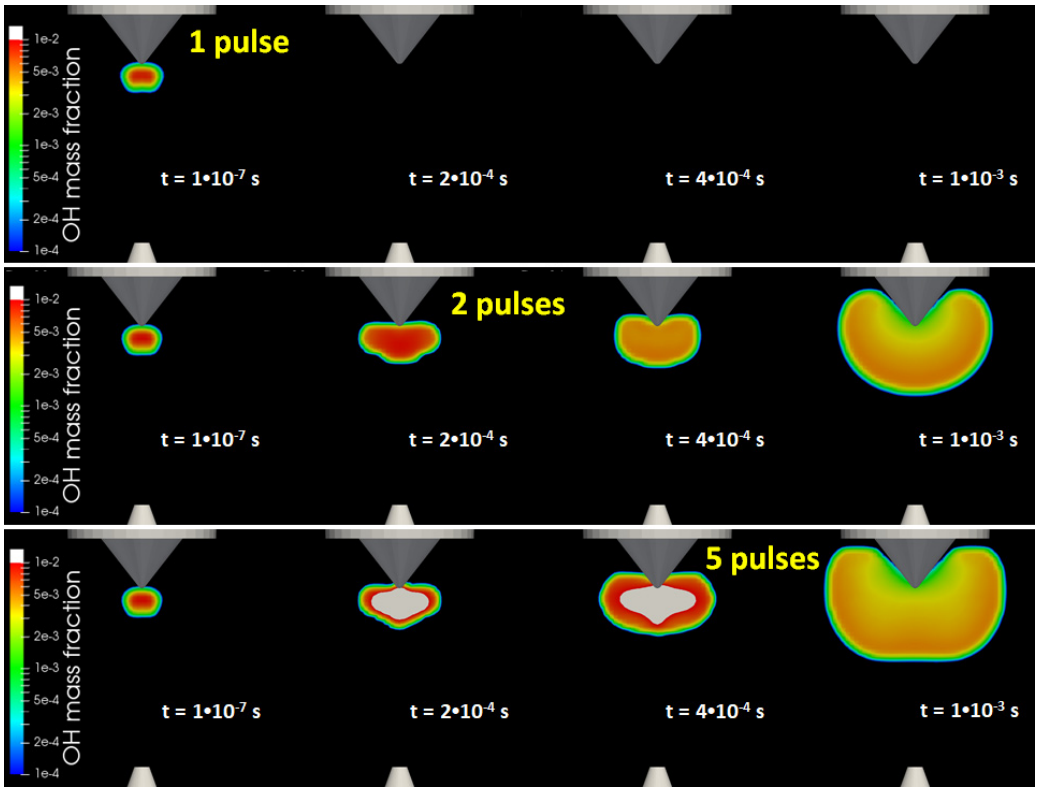


*Figure 8: OH distribution for case 2 (19 kV, 2.0 bar) for 1, 2, and 5 pulses*

## 3 Conclusions

This paper leveraged multi-dimensional simulations to investigate the characteristics of non-equilibrium plasma generated by nanosecond pulsed high-voltage discharge in a pin-to-pin electrode configuration. The goal of this study was to evaluate the post-discharge thermal and chemical plasma properties and their impact on LTP ignition processes. Main conclusions can be listed as follows:

- Non-equilibrium plasma simulations correctly predicted the evolution of the streamer discharge in the gap between the electrodes, and the resulting discharge output for a single-pulse discharge, that was experimentally observed to be in the glow regime.
- Simulation results closely matched two key quantities, namely atomic oxygen and temperature, measured in optically accessible calorimetry for a single-pulse discharge. In particular, simulations well matched the quantity of ground state atomic oxygen measured in experiments via O-TALIF at the same location.
- The impact of both types of deposition, i.e. thermal and non-thermal, was evaluated using CFD in a multi-pulse fashion. Results, not shown in this paper, highlighted that at such deposition values, the chemical component is the most important one.
- CFD combustion simulations showed the impact of the number of pulses on the LTP ignition mechanism. A minimum number of pulses was identified to trigger ignition successfully for each case. Non-stoichiometric mixture and the presence of non-quiescent flow will likely alter the number of pulses required for successful LTP ignition.

## Acknowledgments

The submitted manuscript has been created by UChicago Argonne, LLC, Operator of Argonne National Laboratory (“Argonne”). Argonne, a U.S. Department of Energy Office of Science laboratory, is operated under Contract No. DE-AC02-06CH11357. The U.S. Government retains for itself, and others acting on its behalf, a paid-up nonexclusive, irrevocable worldwide license in said article to reproduce, prepare derivative works, distribute copies to the public, and perform publicly and display publicly, by or on behalf of the Government.

This research is funded by DOE's Vehicle Technologies Program, Office of Energy Efficiency and Renewable Energy. The authors would like to express their gratitude to Gurpreet Singh and Mike Weismiller, program managers at DOE, for their support. Numerical simulations were run on the Bebop Cluster at the LCRC facility, Argonne National Laboratory.

## Literature

[1] Takahashi, D., Nakata, K., Yoshihara, Y., Ohta, Y. et al., "Combustion Development to Achieve Engine Thermal Efficiency of 40% for Hybrid Vehicles," SAE Technical Paper 2015-01-1254, 2015.

[2] Ikeya, K., Takazawa, M., Yamada, T., Park, S. et al., "Thermal Efficiency Enhancement of a Gasoline Engine," SAE Int. J. Engines 8(4):1579-1586, 2015.

[3] Briggs, T., Alger, T., and Mangold, B., "Advanced Ignition Systems Evaluations for High-Dilution SI Engines," SAE Int. J. Engines 7(4):1802-1807, 2014.

[4] Sevik, J., Wallner, T., Pamminger, M., Scarcelli, R., et al., “Extending Lean and Exhaust Gas Recirculation-Dilute Operating Limits of a Modern Gasoline Direct-Injection Engine Using a Low-Energy Transient Plasma Ignition System,” J. Eng. Gas Turbines Power 138(11):112807, 2016.

[5] Starikovskaia, S.M., “Plasma-assisted ignition and combustion: nanosecond discharges and development of kinetic mechanisms,” J. Phys. Appl. Phys. 47(35):353001, 2014.

[6] Aleksandrov, N. L., Kindysheva, S. V., Kosarev, I. N., Starikovskaia, S. et al., “Mechanism of ignition by non-equilibrium plasma”, Proc. Combust. Inst. 32 205–12, 2009.

[7] VizGlow User Manual v2.2, Esgee Technologies Inc., Austin, Texas, USA,, http://esgeetech.com/

[8] Anqi Zhang et al 2018 J. Phys. D: Appl. Phys. 51 345201.

[9] Richards, K.J., Senecal, P.K., Pomraning, E., CONVERGECFD 2.3.0 Theory Manual, Convergent Science Inc., Madison, WI, 2016.

[10] Givler, S.D., Raju, M., Pomraning, E., Senecal, P.K., Salman, N., Reese II, R.A., “Gasoline Combustion Modeling of Direct and Port-Fuel Injected Engines, using a Reduced Chemical Mechanism”, SAE Technical Paper 2013-01-1098, 2013.

[11] Dan Singleton et al 2011 J. Phys. D: Appl. Phys. 44 022001.